SUPPRESSION CHARACTERISTICS OF CUP-BURNER FLAMES IN LOW GRAVITY

Fumiaki Takahashi
National Center for Microgravity Research on Fluids and Combustion
NASA Glenn Research Center
Cleveland, OH 44135

Gregory T. Linteris
Fire Research Division, National Institute of Standards and Technology
Gaithersburg, MD 20899

Viswanath R. Katta
Innovative Scientific Solutions Inc.
Dayton, OH 45440

ABSTRACT·

The structure and suppression of laminar methane-air co-flow diffusion flames formed on a cup burner have been studied experimentally and numerically using physically acting fire-extinguishing agents (CO_2, N_2, He, and Ar) in normal earth ($1g$) and zero gravity ($0g$). The computation uses a direct numerical simulation with detailed chemistry and radiative heat-loss models. An initial observation of the flame without agent was also made at the NASA Glenn 2.2-Second Drop Tower. An agent was introduced into a low-speed coflowing oxidizing stream by gradually replacing the air until extinguishment occurred under a fixed minimal fuel velocity. The suppression of cup-burner flames, which resemble real fires, occurred via a blowoff process (in which the flame base drifted downstream) rather than the global extinction phenomenon typical of counterflow diffusion flames. The computation revealed that the peak reactivity spot (the reaction kernel) formed in the flame base was responsible for attachment and blowoff of the trailing diffusion flame. The extinguishing agent volume fractions determined experimentally in $1g$ were CO_2, 15.7±0.6 %; N_2, 25.9±1.0 %; He, 26.7±1.1 %; and Ar, 37.3±1.5 %. The numerical simulation performed thus far predicted the extinguishing agent volume fractions as: CO_2, 14.5 % (or 16.1 % with different kinetic parameters for a methyl-H atom reaction step) in $1g$ and CO_2, 19.1 %; N_2, ≈38 %; He, 30.7 %; and Ar, ≈49 % in $0g$. The buoyancy-induced flame flickering in $1g$ and thermal and transport properties of the agents affected the flame extinguishment limits.

INTRODUCTION

In the exploration and development of space, long-duration missions increase a likelihood of fire events. Although controlling the flammability of materials aboard spacecraft is an essential approach, we must be prepared for a worst case scenario in which an accidental fire must be suppressed. Fire-extinguishing agents act to suppress the flame physically and/or chemically[1]. Examples of physically acting agents are carbon dioxide (CO_2) and water-based foam used in the International Space Station as well as numerous terrestrial applications. However, these chemically passive agents are relatively inefficient as fire suppressants[2,3]. The chemically active agent, halon 1301 (CF_3Br), which is still in use in the Space Shuttle, is highly effective, but its production was banned by the Montreal Protocol[4,5] in 1995. Although the existing systems may continue to be used, new agents or techniques are ultimately needed for long-duration missions[3,6]. Despite their less effectiveness as fire-extinguishing agents, physically acting agents are more likely to be used for space applications for safety reasons. Furthermore, fire behavior and suppression in the missions are strongly influenced by low-gravity environments in flight and on the planetary surfaces;

and thus fire safety technology must be tailored to respond to the unusual fire characteristics in low-gravity environments[2]. Therefore, the flame structure and underlying physics of suppression phenomena in low gravity, particularly using physically acting fire-extinguishing agents, are of relevant importance in space fire safety.

For testing the effectiveness of fire-extinguishing agents, the industry-standard cup burner apparatus[7] is most widely used[8-23] in fire safety engineering. The cup-burner flame is a laminar co-flow diffusion flame with a circular fuel source (2.8 cm diameter, either a liquid pool or a low-velocity gas jet) inside a co-axial chimney with an oxidizer flow. An agent is generally introduced into the coflowing oxidizer in the cup-burner system to determine the critical agent concentration at extinguishment. The cup-burner flame resembles a real fire, which consists of flame segments subjected to various strain rates, including stabilized or spreading edge (base) of diffusion flames, and exhibits flame flickering (and separation) in 1g, affecting the air and agent entrainment into the flame zone. Thus, the cup burner flame serves as a scale model of real fires for evaluating the agent effectiveness. Because of its resemblance to fires, great faith has been placed in agent extinguishment concentrations determined in the cup burner experiment, and many safety codes and design practices are based on the cup-burner values[7]. However, there exists virtually <u>no</u> fundamental understanding of the flame suppression process for this device. Little is known concerning the amount of agent that is transported into various regions of the flame, or whether the extinguishment occurs globally over the flame or in stabilization regions. Clearly, the understanding of fire suppression by physically or chemically acting agents would be greatly improved if their effect in cup-burner flames was investigated from a fundamental perspective.

As a result of significant progresses in the development of detailed combustion reaction mechanisms and computer technologies over the last decade or two, it is now feasible to simulate various transient combustion phenomena in simple configurations (burner geometry, flow, and fuel) with confidence, leading to deeper understanding of physical and chemical unit processes taking place during the phenomena under investigation. In recent years, the authors have investigated[24-32] the dynamic behavior of diffusion flames, internal flame structure, including radical transport and reactions, extinction processes, blowoff/liftoff phenomena, and physical and chemical flame suppression processes. The overall objectives of the present study are to understand the physical and chemical processes of cup-burner flame suppression phenomena and to provide rigorous testing of

numerical models, which include detailed chemistry and radiation sub-models. In this paper, the experimental and numerical results of the structure of the flame stabilizing region and the extinguishment limits are reported using methane as the fuel and physically acting gaseous agents (N_2, He, and Ar) in addition to CO_2, studied previously[30,31].

EXPERIMENTAL PROCEDURES

The cup burner, described previously[11], consists of a cylindrical glass cup (28 mm diameter, burner rim chamfered inside) positioned inside a glass chimney (8.5 cm or 9.5 cm diameter, 53.3 cm height). To provide uniform flow, 6 mm glass beads fill the base of the chimney, and 3 mm glass beads (with two 15.8 mesh/cm screens on top) fill the fuel cup. Gas flows were measured by mass flow controllers (Sierra 860[*]) which were calibrated so that their uncertainty is 2 % of indicated flow. The burner rim temperature, measured at 3.7 mm below the exit using a surface temperature probe after running the burner for ≈10 minutes, was (514 ± 10) K.

The fuel gas used is methane (Matheson UHP, 99.9 %), and the agents are carbon dioxide (Airgas, 99.5 %), nitrogen (boil-off), helium (MG Ind., 99.95 %), and argon (MG Ind., 99.996 %). The air is house compressed air (filtered and dried) which is additionally cleaned by passing it through an 0.01 μm filter, a carbon filter, and a desiccant bed to remove small aerosols, organic vapors, and water vapor. To determine the suppression condition, for a fixed methane flow rate (0.34 L/min which converts to the mean fuel velocity of 0.92 cm/s), the agent was added (in increments of < 1 % near extinction) to co-flowing air (held at a constant flow rate) until extinguishment occurred. The test was repeated at least three times at different mean coflow velocities.

An uncertainty analysis was performed, consisting of calculation of individual uncertainty components and root mean square summation of components. All uncertainties are reported as *expanded uncertainties*: $X \pm ku_c$, from a combined standard uncertainty (estimated standard deviation) u_c, and a coverage factor $k = 2$. Likewise, when reported, the relative uncertainty is ku / X. The expanded relative uncertainties for the experimentally determined quantities in this study are: the volume fractions of CO_2, N_2, He, and Ar: 4 % for each.

---

[*]Certain commercial equipment, instruments, or materials are identified in this paper to adequately specify the procedure. Such identification does not imply recommendation or endorsement by NIST, nor does it imply that the materials or equipment are necessarily the best available for the intended use.

NUMERICAL METHODS

A time-dependent, axisymmetric numerical code (UNICORN[33]) is used for the simulation of unsteady jet diffusion flames stabilized on the cup burner. The code solves the axial and radial (z and r) full Navier-Stokes momentum equations, continuity, and enthalpy- and species-conservation equations on a staggered-grid system. The body-force term due to the gravitational field is included in the axial-momentum equation to simulate upward-oriented flames. A clustered mesh system is employed to trace the gradients in flow variables near the flame surface. A detailed reaction mechanism of GRI-V1.2[34] for methane-oxygen combustion (31 species and 346 elementary reactions) is incorporated into UNICORN. Thermophysical properties of species are calculated from the polynomial curve fits for 300 - 5000 K. Mixture viscosity and thermal conductivity are then estimated using the Wilke and Kee expressions, respectively. A simple radiative heat-loss model[35] based on optically thin-media assumption and Plank-mean absorption coefficients for CO_2, H_2O, CH_4, and CO, was incorporated into the energy equation.

The finite-difference forms of the momentum equations are obtained using an implicit QUICKEST scheme[36], and those of the species and energy equations are obtained using a hybrid scheme of upwind and central differencing. At every time-step, the pressure field is accurately calculated by solving all the pressure Poisson equations simultaneously and using the LU (Lower and Upper diagonal) matrix-decomposition technique.

Unsteady axisymmetric calculations for the cup-burner flames are made on a physical domain of 200×47.5 mm using a 251×101 or 541×251 non-uniform grid system that yielded 0.2×0.2-mm or 0.05×0.05-mm minimum grid spacing, respectively, in both the z and r directions in the flame zone. The computational domain is bounded by the axis of symmetry and a chimney wall boundary in the radial direction and by the inflow and outflow boundaries in the axial direction. The boundary conditions are treated in the same way as those reported in earlier papers[30-32]. The outflow boundary in z direction is located sufficiently far from the burner exit (>7 fuel-cup diameters) such that propagation of boundary-induced disturbances into the region of interest is minimal. Flat velocity profiles are imposed at the fuel and air inflow boundaries, while an extrapolation procedure with weighted zero- and first-order terms is used to estimate the flow variables at the outflow boundary.

The cup burner outer diameter is 28 mm and the burner wall is treated as a 1-mm long and 1-mm thick tube. The wall temperature is set at 600 K, which is somewhat higher than the afore-mentioned measurement made below the exit. The fuel and oxidizer velocities are 0.921 cm/s and 10.7 cm/s, respectively. The low fuel velocity represents a condition at which the flame size is comparable to that of typical liquid-fuel cup-burner flames. The air velocity is in the middle of the so-called "plateau region" [7, 10, 14], where the extinguishing agent concentration is independent of the oxidizer velocity.

RESULTS AND DISCUSSION

Figure 1 shows video images of stable cup-burner flames of methane in coflowing air in 1g and μg. In 1g, the blue flame base anchored at the burner rim, and the downstream portion of the flame contracted inwardly, and had an orange-yellow tip due to soot formation. The flame was dynamic due to flickering. The flickering frequency measured at ≈5 cm above the burner by a photodiode was typically ≈1 Hz or ≈15 Hz, depending on the air velocity. As an agent was added into coflowing air, the entire flame turned blue. As the agent concentration was increased to the suppression limit, the flame base oscillated just before the flame blew off.

A preliminary observation of a methane cup-burner flame without agent was made at the NASA Glenn 2.2-Second Drop Tower. A video image of the μg flame is shown in Fig. 1b (the intensity is substantially enhanced to improve visibility). In μg, the blue flame
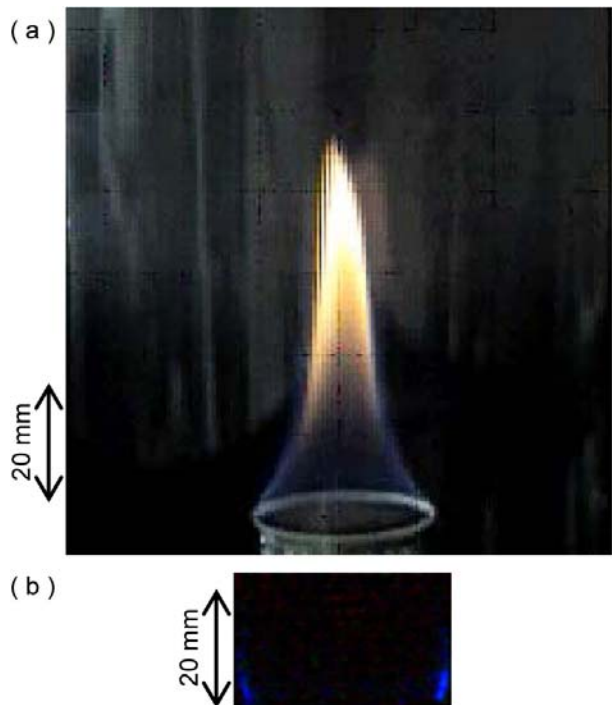

Fig. 1 Video images of methane cup-burner flames in air. (a) 1g, (b) μg. $U_{CH4} = 0.92$ cm/s, $U_{ox} = 10.7$ cm/s.

attached to the outer edge of the burner rim and the downstream portion appeared to be extinguished, thus opening the flame tip. This observation validates the numerical prediction performed previously[31].

Figure 2 shows the critical agent volume fraction in the oxidizer at extinguishment for 1g flames. The critical values were nearly independent of the oxidizer velocity over the range tested. This insensitivity of the suppression limit to the oxidizer flow, once a minimum flow is achieved, in a so-called "plateau region" has been reported in the literature[7,10,14]. The fuel velocity, the fuel cup diameter, and the chimney diameter are also known to have a small or negligible impact on the agent concentration at suppression[10]. Nonetheless, the extinction volume fraction increases mildly with the oxidizer velocity for CO_2, N_2, and Ar, but decreases mildly for He. Table 1 lists the extinguishing volume fractions of each agent determined from the plateau region, the limiting oxygen volume fractions, and the adiabatic flame temperature[37] at the stoichiometric fuel-oxidizer mixture with the indicated extinguishing agent concentration. The limiting oxygen volume fractions were converted from the extinguishing volume fractions as $X_{O2} = 0.209(1 - X_{agent})$ where X_{O2} = the oxygen volume fraction and X_{agent} = the agent volume fraction. The descending order of the agent effectiveness is $CO_2 > N_2 \approx He > Ar$. The adiabatic flame temperatures at the extinguishment limits for CO_2, N_2, and Ar are relatively low and close each other, indicating that the dilution and thermal effects lowered the temperatures and, in turn, the overall reaction rates toward the limits. In fact, the descending order of the molar specific heats is $CO_2 > N_2 > He = Ar$. Thus, the CO_2 took away heat from the flame most effectively and the extinguishment limit was reached at the lowest volume fraction. The adiabatic flame temperature at the extinguishment limit for helium is much higher than the others, suggesting that there may be additional effects. An apparent difference in transport properties is the thermal conductivity of helium, which is several times greater than those of the others. Thus, dilution with helium increases the thermal conductivity of the gas mixture and may have contributed to dissipate heat more effectively.

Figure 3 shows the calculated structure of a methane flame in air in 1g, including the velocity vectors (**v**), isotherms (T), and total heat-release rate ($\dot{q}$). Although flickering and soot formation complicate comparisons of the observed visual flame shape with those from the calculations, a preliminary assessment shows them to be consistent. The velocity vectors show the longitudinal acceleration in the hot zone due to buoyancy. As a result of the continuity of the fluid, surrounding air was entrained into the lower part of the flame. The entrainment flow inclined inwardly because of the minimal fuel flow rate. The heat-release rate contours show the reaction kernel (peak reactivity spot, $\dot{q}_k$ = 148 J/cm^{3}s) at the flame base. The velocity and temperature at the reaction kernel were $|v_k|$ = 0.304 m/s and T_k = 1511 K, respectively. The reactivity decreased in downstream portions of the flame because of dilution of the reactants by nitrogen and the combustion products, whereas the velocity increased downstream by a cumulative effect of the buoyancy-induced flow. Thus, the vigorously burning reaction kernel sustained stationary combustion processes in the flow and held the trailing flame (as has been revealed for methane jet diffusion flames previously[25-28]).

Figure 4 shows the variations of the temperature, species mole fractions (X_i), formation rates ($\hat{\omega}_i$), and total heat-release rate across the reaction kernel of the 1g flame in air. General trends in the species mole fractions and formation rates resembled to those in the methane-air co-flow jet diffusion flames studied previously (Fig. 9 in Ref. 26), in which more leakage of the fuel and oxygen occurred through the larger stand-off distance of the flame base from the jet exit. Basic features in the flame structure are typical of diffusion flames; i.e., chain radicals formed at high temperatures
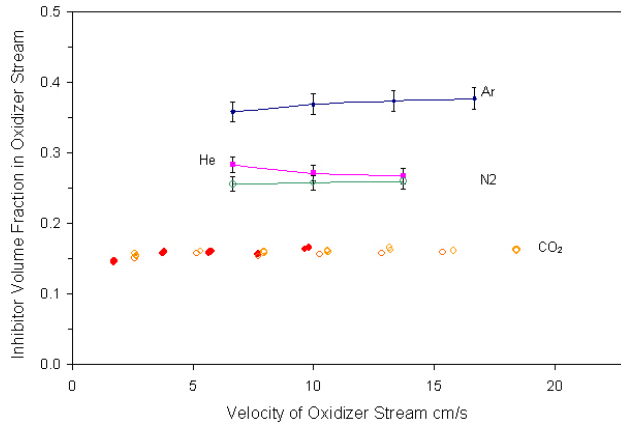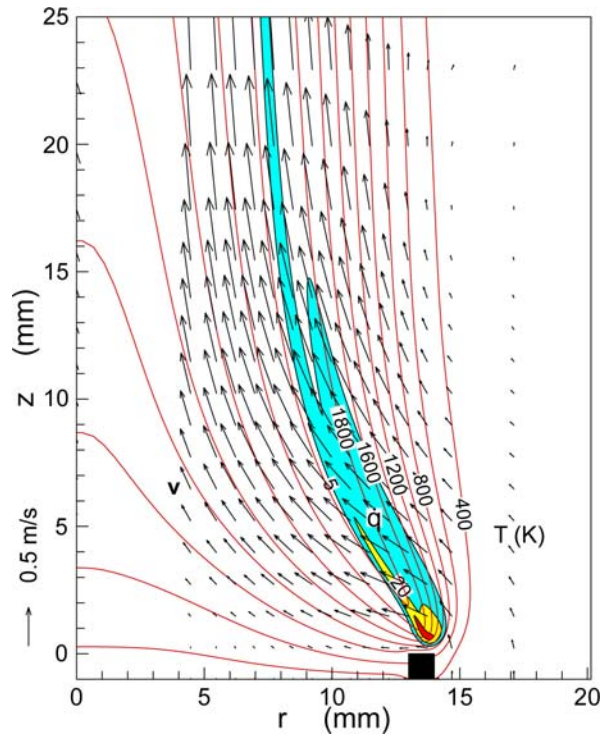

Fig. 2   Effects of the oxidizer velocity on the critical agent volume fraction at extinguishment.

Table 1 Extinguishment Limit and Adiabatic Flame Temperature

Agent	Extinguishing Agent Volume Fraction (%)	Limiting O_2 Volume Fraction (%)	Adiabatic Flame Temperature (K)
CO_2	15.7±0.6	17.6±0.1	1927
N_2	25.9±1.0	15.5±0.2	1900
He	26.7±1.1	15.3±0.2	2001
Ar	37.3±1.5	13.1±0.2	1875

Fig. 3 Calculated structure of a methane cup-burner flame in air in $1g$. $\dot{q}$ contours: 5, 20, and 80 J/cm^{3}s.

on the air side (slightly) of the peak reaction zone dissociate and pyrolyze the fuel into hydrocarbon fragments and C_2 species on the fuel side (slightly); H_2 and CO are oxidized to products on the air side. Distinct exceptions are that the oxygen penetrated onto the fuel side through the quenched space, thus resulting in high oxygen concentration around the reaction kernel and that the fuel escaped through the quenched space onto the air side, thus making a small hump in the mole fraction curve. The heat-release rates of elementary steps (not shown) revealed that the methyl oxidation reaction, $CH_3 + O \rightarrow CH_2O + H$ (R19), and the final product formation, $H_2 + OH \rightarrow H_2O + H$ (R165), were major contributors ($\approx$58%) to the total heat-release rate peak. The reaction rates of elementary steps (not shown) indicated that the chain-branching, $H + O_2 \rightarrow OH + O$ (R73), was the fastest reaction of all, with its peak reaction rate coincident with the heat-release rate peak. Other fast reactions were the fuel dehydrogenation, $CH_4 + OH \rightarrow CH_3 + H_2O$ (R191) and $CH_4 + H \rightarrow CH_3 + H_2$ (R103), on the fuel side, the methyl oxidation (R19) at the heat-release rate peak, and the final product formation, (R165) and $CO + OH \rightarrow CO_2 + H$ (R193) on the air side.
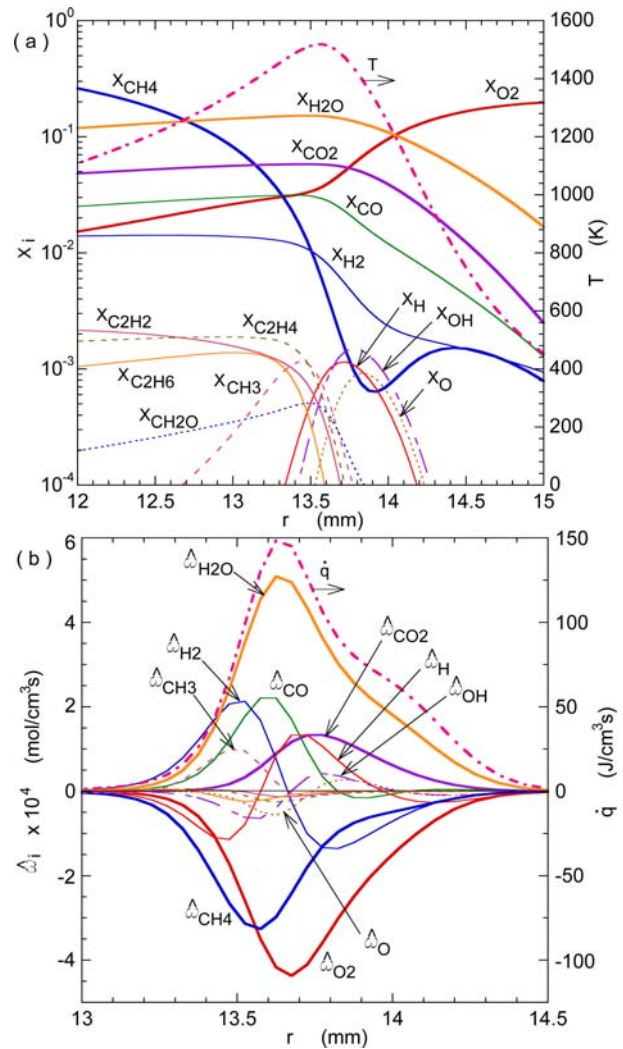

Fig. 4 Variations of the calculated variables across the reaction kernel of a methane flame in air in $1g$. z_k = 1.78 mm. (a) Temperature and mole fractions, (b) heat-release rate and production rate of species i.

Figure 5 shows the calculated structure of a methane flame in air in $0g$. The location and size of the higher reactivity ($\dot{q}_k$ > 10 J/cm^{3}s) portion of the simulated flame were consistent with the observed blue flame (Fig. 1b).

Because of lack of buoyancy, the velocity vectors show only slight acceleration in the hot zone due to thermal expansion. As the momentum of the coflowing air transferred to the low-speed wake-like region behind the cup burner, the velocity distribution became nearly uniform downstream. The flame zone was formed nearly vertically, and the surrounding air came into the lower part of the flame. These overall trends resembled to those of the jet diffusion flame in the coflow (0.12 m/s) air in $0g$ previously studied (Fig. 6 in
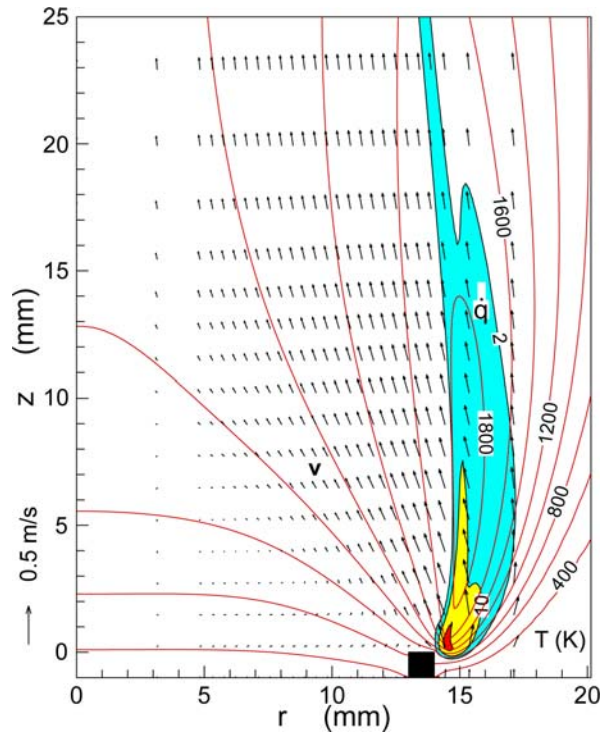
Fig. 5 Calculated structure of a methane cup-burner flame in air in 0g. $\dot{q}$ contours: 2, 10, and 50 J/cm^{3}s.
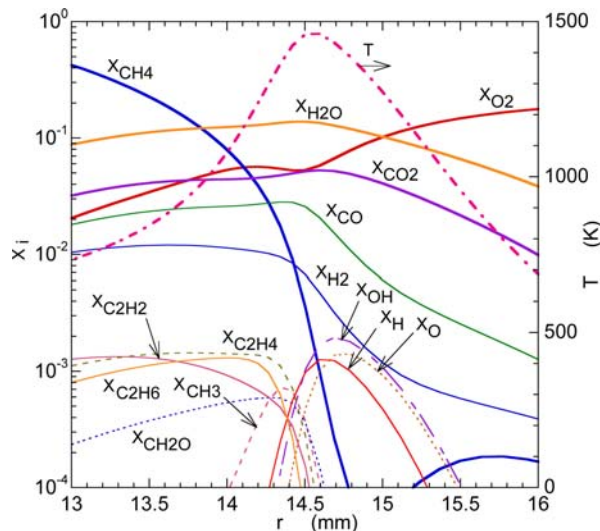

Fig. 6 Variations of the calculated temperature and mole fractions across the reaction kernel of a methane flame in air in 0g. $z_k = 1.3$ mm.

Ref. 28). Figure 6 shows the variations of the temperature and species mole fractions across the reaction kernel of the 0g flame. The flame structure is similar to that of the 1g flame (Fig. 4), except for the methane mole fraction showing much less leakage

through the quenched space and the reaction zone broadening on the air side due to significantly weaker inward flow entrainment.

Figure 7 shows how increasing the volume fraction of agent in the air stream (X_{agent}) affects the radial and axial position of the peak reaction spot and its temperature, as well as the velocity of the gases passing the reaction kernel. As the agent fraction was increased, the axial stand-off distance of the reaction kernel increases gradually for $X_{agent} > 0.15$ and then more steeply as X_{agent} approaches the extinguishment limit. For each incrementally larger agent volume fraction in the simulation, a steady-state solution for a stable stationary flame was obtained, which showed a larger reaction kernel stand-off distance. In other words, the extinguishment occurred as a result of the blowoff process rather than the global extinction phenomenon typical of counterflow diffusion flame. This finding is of practical importance in fire suppression because fire spread over condenced fuel surfaces and extinguishment of such fires must relate to the attachement and blowoff processes of diffusion flames with edges (bases) as represented by the cup-burner flame. During the blowoff process caused by dilution with the inert gas, the reaction kernel temperature decreased modelately, whereas the velocity and the heat-release rate (not shown) decreased more substantially. This result suggests that the reaction kernel shifted downstream to seek a location where the residence time (which depends on the reciprocal of the velocity) is sufficient for the longer chemical reaction time (which depends on the reciprocal of the reactivity) caused by dilution. Therefore, the overall mechanism of the flame-base movement must be based on the subtle balance between the chemical time and the residence time. This reaction kernel hypothesis [27] has been proposed for the lifting process of jet diffusion flames as a result of an increase in the coflowing air velocity. However, unlike the dilution process in the present case, increasing the coflowing air velocity increased the peak reactivity (i.e., the "blowing effect") and pushed the reaction-kernel downstream at an increased velocity.

For helium, the flame extinguished if the agent volume fraction was increased to 30.7 %. The flame base oscillated before extinguishment. For nitrogen and argon, the reaction-kernel stand-off distance continued to increase with the agent volume fraction. Thus, for a practical reason, the computation was stopped when the stand-off distance became substantially large ($z_k > 30$ mm), and the extinguishment agent volume fractions were determined by drawing asymptotes as N$_2$, $\approx$38 %; and Ar, $\approx$49 %. Although the experimental results in μg have not yet been available, the order of the predicted
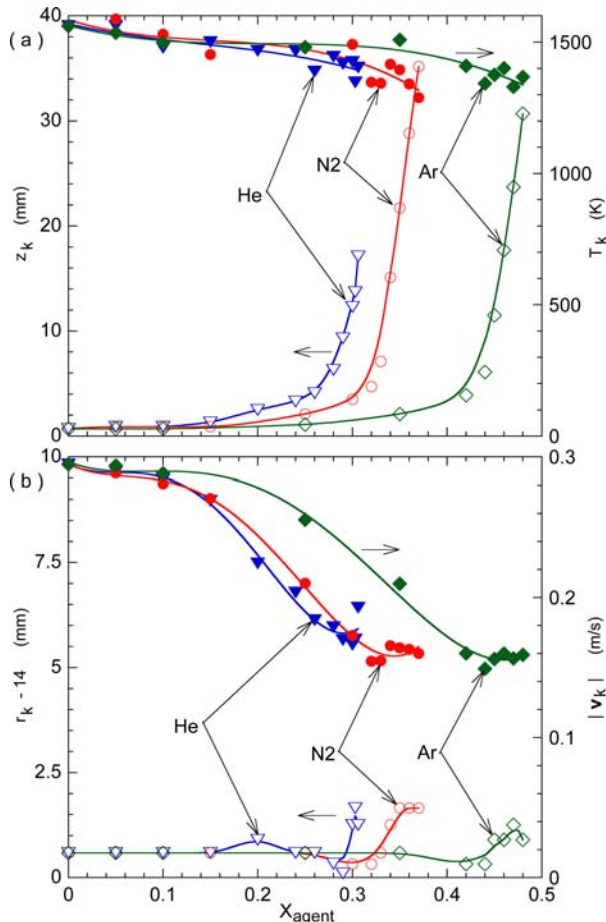
Fig. 7 Variations of the reaction kernel coordinates, temperature, and velocity as a function of the agent volume fraction.

data is consistent with the measurements in 1g, except for the reversed order of nitrogen and helium. Thermal and transport properties of agents affected the extinguishment limits. The molar specific heat of carbon dioxide is 1.3 times larger than that of nitrogen and 1.8 times larger than those of helium and argon (at 300 K), thus taking heat from the flame most effectively. The thermal conductivity of helium is 9 times larger than that of carbon dioxide, thus dissipating heat from the reaction kernel more effectively. The extinguishment limits in 0g tend to be substantially higher than those in 1g. A possible explanation is the effect of the buoyancy-induced flow and flickering, which caused disturbances in the reaction kernel flow velocity and species concentration fields, thus breaking the subtle local balance and triggering flame blowoff.

Figure 8 shows the calculated structure of a methane flame in 0 g, with and oxidizer of 64 % air and 34 % added nitrogen. The figure shows the velocity vectors, isotherms, total heat-release rate, and local
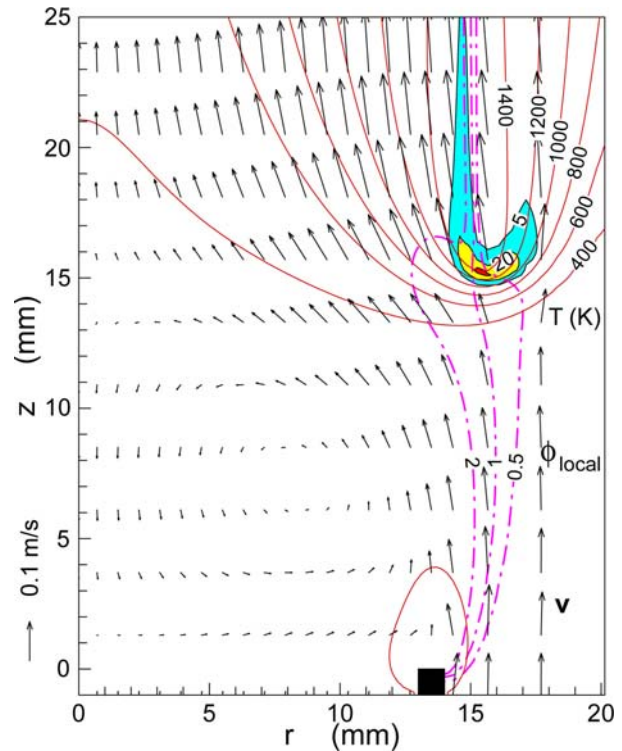

Fig. 8 Calculated structure of a methane cup-burner flame in 66 % air/34% N_2 in 0g. $\dot{q}$ contours: 5, 20, and 80 J/cm³s.

equivalence ratio (ϕ_{local}). The local equivalence ratio, defined by considering a stoichiometric expression for intermediate species in the mixture to be converted to CO_2 and H_2O, is identical to the conventional equivalence ratio in the unburned fuel-air mixture. The gas velocity increases in the hot zone due to thermal expansion and is directed toward the low-speed wake behind the cup burner, thus forming a recirculation zone. The fuel-oxidizer mixing occurred over the stand-off distance of ≈15 mm, which converts to the residence time of ≈0.15 s. The heat-release rate contours show a hook-shaped flame base with the reaction kernel, which resembles to that in jet diffusion flames in coflowing air in 1g studied previously[26,27].

Figure 9 shows the variations of the temperature and species mole fractions across the reaction kernel of the 0g flame in the oxidizer of 64 % air and 34 % added nitrogen. The high nitrogen mole fraction shows the highly diluted reaction zone. The large stand-off distance and relatively low velocity resulted in substantial fuel-oxidizer mixing, forming a flammable mixture layer upstream the flame base. As a result of the vigorously burning reaction kernel inside the incoming flammable mixture flow, the radial distributions of the species mole fractions show a unique flame structure, where the fuel-side variations
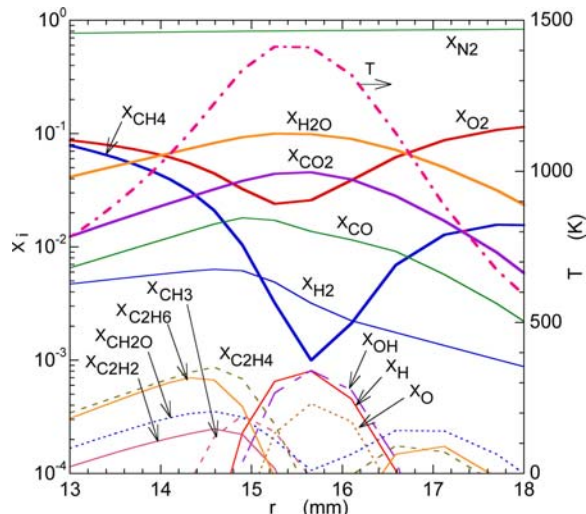
Fig. 9   Variations of the calculated temperature and mole fractions across the reaction kernel of a methane flame in 66 % air/34% N_2 in 0g. z_k = 16.3 mm.

are somewhat mirrored on the air side with the leftover fuel. This trend was observed previously[29] in the edge diffusion flame propagating through the flammable mixture layer in the fuel jet.

CONCLUSIONS

The laboratory experiment and direct numerical simulations have revealed the structure and suppression behavior of laminar methane-air co-flow diffusion flames formed in the cup-burner configuration under 1g and 0g conditions. In 1g, the buoyancy-induced flow acceleration in the hot region downstream resulted in the inward air entrainment into the wake behind the cup burner, thus inclining the diffusion flame inwardly with the edge (base) of the flame being attached to the burner rim. In 0g, the tip of the flame extinguished (thus opened), and the short flame anchored at the outer edge of the burner rim. In both 1g and 0g, a peak reactivity spot (the reaction kernel) was formed in the flame stabilizing region, thus holding the trailing diffusion flame. As the physically acting fire-extinguishing agent was introduced into the coflowing oxidizer, the flame base detached from the burner rim and drifted downstream. Thus, the suppression of cup-burner flames occurs via a blowoff process rather than the global extinction phenomenon typical of counterflow diffusion flames. The extinguishing agent volume fraction determined experimentally in 1g were CO_2, 15.7±0.6 %; N_2, 25.9±1.0 %; He, 26.7±1.1 %; and Ar, 37.3±1.5 %.   The numerically predicted extinguishing agent volume fractions are CO_2: 14.5 % (or 16.1 % with different kinetic parameters for a methyl-H atom reaction step) in 1g and CO_2, 19.1 %;

N_2, ≈38 %; He, 30.7 %; and Ar, ≈49 % in 0g. Therefore, the 1g flames are in general more easily be extinguished because disturbances by the buoyancy-induced flow and flickering tend to trigger flame blowoff. Thermal and transport properties of agents affects the extinguishment limits; i.e., the high molar specific heat of carbon dioxide takes heat from the flame effectively and the high thermal conductivity of helium dissipates heat from the reaction kernel effectively.

REFERENCES

1. Sheinson, R. S., Pener-Hahn, J. E., and Indritz, D., The Physical and Chemical Action of Fire Suppressants, *Fire Safety Journal,* 15, 437-450 (1989).

2. Friedman, R., Fire Safety in Extraterrestrial Environments, NASA/TM-1998-207417, 1998.

3. Friedman, R., and Ross, H. D., Combustion Technology and Fire Safety for Human-crew Space Missions, In *Microgravity Combustion: Fire in Free Fall* (H. D. Ross Ed.), Academic Press, San Diego, 2001, p.83.

4. Grosshandler, W. L., Gann, R. G., and Pitts, W. M., (eds.), Evaluation of Alternative In-Flight Fire Suppressants for Full-Scale Testing in Simulated Aircraft Engine Nacelles and Dry Bay, SP 861, National Institute of Standards and Technology, 1994.

5. Harrison, G. C., Halon Replacement in Aircraft and Industrial Applications, In *Halon Replacements: Technology and Science* (A. W. Miziolec and W. Tsang, Eds.), American Chemical Society, Washington, DC, 1995, pp. 74-84.

6. Annon., Workshop on Research for Space Exploration: Physical Sciences and Process Technology, NASA/CP-1998-207431, May 1998.

7. National Fire Protection Agency, *Standard on Clean Agent Fire Extinguishing Systems,* NFPA 2001, 1994.

8. Bajpai, S. N., An Investigation of the Extinction of Diffusion Flames by Halons, *Journal of Fire and Flammability,* 5, 255 (1974).

9. Hirst, R., and Booth, K., Measurements of Flame-Extinguishing Concentrations, *Fire Technology,* 13, 4 (1977).

10. Hamins, A., Gmurczyk, G., Grosshandler, W., Rehwoldt, R. G., Vazquez, I., Cleary, T., Presser, C., and Seshadri, K., Flame Suppression

Effectiveness, *Evaluation of Alternative In-Flight Fire Suppressants for Full-Scale Testing in Simulated Aircraft Engine Nacelles and Dry Bays* (W. L. Grosshandler, R. G. Gann, and W. M. Pitts, Eds.), National Institute of Standards and Technology, NIST SP 861, 1994, pp. 345-465.

11. Linteris, G. T. and Gmurczyk, G. W., in *Fire Suppression System Performance of Alternative Agents in Aircraft Engine and Dry Bay Laboratory Simulations* (R.G. Gann, Ed.), National Institute of Standards and Technology, NIST SP 890, Gaithersburg, MD, 1995, pp. 201-318.

12. Sakai, R., Saito, N., Saso, Y., Ogawa, Y., and Inoue, Y., Flame Extinguishing Concentrations of Halon Replacements for Flammable Liquids, Report of Fire Research Institute of Japan, No. 80, 1995, pp. 36-42.

13. Moore, T. A., Weitz, C. A., and Tapscott, R. E., An update of NMERI Cup-Burner Test Results, Proceedings of the 6th Halon Options Technical Working Conference (HOTWC-96), Albuquerque, NM, 1996, pp. 551-564.

14. Moore, T. A., Martinez, A., and Tapscott, R. E., A Comparison of the NMERI and ICI-style Cup-Burners, Proceedings of the 7th Halon Options Technical Working Conference (HOTWC-97), Albuquerque, NM, 1997, pp. 388-395.

15. Saito, N., Ogawa, Y., Saso, Y., and Sakai, R., Improvement on Reproducibility of Flame Extinguishing Concentration Measured by Cup Burner Method, Report of Fire Research Institute of Japan, No. 81, 1996, pp. 22-29.

16. Senecal, J. A., Cup-burner Extinguishing Concentration Correlation with C_1-C_8 class B fuel properties, Proceedings of the 8th Halon Options Technical Working Conference (HOTWC-98), Albuquerque, NM, 1998, pp. 70-79.

17. Babb, M., Gollahalli, S. R., and Sliepcevich, C. M., Extinguishment of Liquid Heptane and Gaseous Propane Diffusion Flames, *Journal of Propulsion and Power,* 15, 260-265 (1999).

18. Tsuji, H., Counter flow diffusion flames. *Progress in Energy and Combust. Sci.,* 8, 93-119 (1982).

19. Simmons, R. F., and Wolfhard, H. G., Some Limiting Oxygen Concentrations for Diffusion Flames in Air Diluted with Nitrogen, *Combustion and Flame,* 1, 155-161 (1957).

20. Hamins, A., Trees, D., Seshadri, K., and Chelliah, H. K., Extinction of Nonpremixed Flames with Halogenated Fire Suppressants, *Combustion and Flame,* 99, 221-230 (1994).

21. Saso, Y., Saito, N., Liao, C., and Ogawa, Y., Extinction of Counterflow Diffusion Flames with Halon Replacements, *Fire Safety Journal,* 26, 303-326 (1996).

22. Papas, P., Fleming, J. W., and Sheinson, R. S., Extinction of Non-premixed Methane- and Propane-Air Counterflow Fames Inhibited with CF_4, CF_3H and CF_3Br, *Proceedings of The Combustion Institute,* Vol. 26, 1996, pp. 1405-1411.

23. Pitts, W. M., and Blevins, L. G., An Investigation of Extinguishment by Thermal Agents using Detailed Chemical Modeling of Opposed-flow Diffusion Flames, Proceedings of the 9th Halon Options Technical Working Conference (HOTWC-99), Albuquerque, NM, 1999, pp. 145-156.

24. Takahashi, F., Schmoll, W. J., Strader, E. A., and Belovich, V. M., Suppression of a Nonpremixed Flame Stabilized by a Backward-Facing Step, *Combustion and Flame,* 122, 105-116 (2000).

25. Takahashi, F., Schmoll, W. J., and Katta, V. R., Attachment Mechanisms of Diffusion Flames, *Proceedings of The Combustion Institute,* Vol. 27, 1998, pp. 675-684.

26. Takahashi, F., and Katta, V. R., Chemical Kinetic Structure of the Reaction Kernel of Methane Jet Diffusion Flames, *Combustion Science and Technology,* 155: 243-279 (2000).

27. Takahashi, F., and Katta, V. R., A Reaction Kernel Hypothesis for the Stability Limit of Methane Jet Diffusion Flames, *Proceedings of The Combustion Institute,* Vol. 28, 2000, pp. 2071-2078.

28. Takahashi, F., and Katta, V. R., Reaction Kernel Structure and Stabilizing Mechanisms of Jet Diffusion Flames in Microgravity, *Proceedings of The Combustion Institute,* Vol. 29, 2002, pp. 2509-2518.

29. Takahashi, F., and Katta, V. R., Propagation and Structure of Edge Diffusion Flames in Axisymmetric Hydrocarbon Fuel Jets, 19th International Colloquium on The Dynamics of Explosions and Reactive Systems (ICDERS), Hakone, Japan, July 2003.

30. Katta, V. R., Takahashi, F., and Linteris, G. T., Numerical Investigations of CO_2 as Fire Suppressing Agent, *Fire Safety Science: Proceedings of the Seventh International Symposium* (Ed. D. D. Evans), International Association for Fire Safety Science, 2003, pp. 531-542.

31. Katta, V. R., Takahashi, F., and Linteris, G. T., Suppression of Cup-Burner Flames Using Carbon Dioxide in Microgravity, *Combustion and Flame,* submitted (2003).

32. Linteris, G. T., Katta, V. R., and Takahashi, F., Experimental and Numerical Evaluation of Metallic Compounds for Suppressing Cup-Burner Flames, *Combustion and Flame,* submitted (2003).

33. Roquemore, W. M., and Katta, V. R., Role of Fow Visualization in the Development of UNICORN,

Journal of Visualization, Vol. 2, No. 3/4, 257-272 (2000).

34. Frenklach, M., Wang, H., Goldenberg, M., Smith, G. P., Golden, D. M., Bowman, C. T., Hanson, R., K., Gardiner, W. C., and Lissianski, V., GRI-Mech—An Optimized Detailed Chemical Reaction Mechanism for Methane Combustion, Technical Report No. GRI-95/0058, Gas Research Institute, Chicago, Illinois, 1995.

35. Annon., Radiation Models, International Workshop on Measurement and Computation of Turbulent Nonpremixed Flames., http://www.ca.sandia.gov/TNF/radiation.html, 2003.

36. Katta, V. R., Goss, L. P., and Roquemore, W. M., Numerical Investigatios of Transitional H_2/N_2 Jet Diffusion Flames, *AIAA Journal,* 32, 84 (1994).

37. McBride, B. J., and Gordon, S., Computer Program for Calculation of Complex Chemical Equilibrium Compositions and Applications—II. Users Manual and Program Description, NASA Reference Publication 1311, June 1996.

American Institute of Aeronautics and Astronautics